ACS NANO

www.acsnano.org

ARTICLE

Hot Carrier-Based Near-Field Thermophotovoltaic Energy Conversion

Raphael St-Gelais,[#,†,‡] Gaurang Ravindra Bhatt,[‡] Linxiao Zhu,[§] Shanhui Fan,[§] and Michal Lipson*[,†,‡]

[†]School of Electrical and Computer Engineering, Cornell University, Ithaca, New York 14853, United States

[‡]Department of Electrical Engineering, Columbia University, New York, New York 10027, United States

[§]Ginzton Laboratory, Stanford University, Stanford, California 94305, United States

ABSTRACT: **Near-field thermophotovoltaics (NFTPV) is a promising approach for direct conversion of heat to electrical power. This technology relies on the drastic enhancement of radiative heat transfer (compared to conventional blackbody radiation) that occurs when objects at different temperatures are brought to deep subwavelength distances (typically <100 nm) from each other. Achieving such radiative heat transfer between a hot object and a photovoltaic (PV) cell could allow direct conversion of heat to electricity with a greater efficiency than using current solid-state technologies (e.g., thermoelectric generators). One of the main challenges in the development of this technology, however, is its incompatibility with conventional silicon PV cells. Thermal radiation is weak at frequencies larger than the ~1.1 eV bandgap of silicon, such that PV cells with lower excitation energies (typically 0.4−0.6 eV) are required for NFTPV. Using low bandgap III−V semiconductors to circumvent this limitation, as proposed in most theoretical works, is challenging and therefore has never been achieved experimentally. In this work, we show that hot carrier PV cells based on Schottky junctions between silicon and metallic films could provide an attractive solution for achieving high efficiency NFTPV electricity generation. Hot carrier science is currently an important field of research and several approaches are investigated for increasing the quantum efficiency (QE) of hot carrier generation beyond conventional Fowler model predictions. If the Fowler limit can indeed be overcome, we show that hot carrier-based NFTPV systems—after optimization of their thermal radiation spectrum—could allow electricity generation with up to 10−30% conversion efficiencies and 10−500 W/cm^2 generated power densities (at 900−1500 K temperatures). We also discuss how the unique properties of thermal radiation in the extreme near-field are especially well suited for investigating recently proposed approaches for high QE hot carrier junctions. We therefore expect our work to be of interest for the field of hot carrier science and—by relying solely on conventional thin film materials—to provide a path for the experimental demonstration of NFTPV energy conversion.**

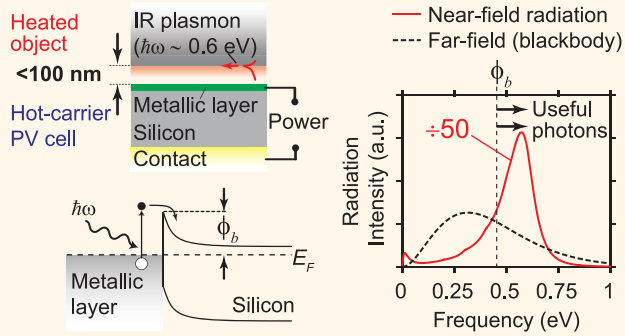

KEYWORDS: *hot carriers, surface plasmon, photovoltaics, energy conversion, thermal radiation, thermophotovoltaics, near-field radiative heat transfer*

Near-field thermo-photovoltaics (NFTPV) is a promising approach for direct conversion of heat to electricity that was the subject of much attention over the last 10 years[1−13] but that still suffers from engineering challenges that so far have prevented its experimental realization. This technology is based on the drastic enhancement of thermal radiation[14−16]—compared to usual Stefan−Boltzmann blackbody radiation—that occurs when objects at different temperatures are brought to very small distances (typically <100 nm) from each other. If at least one of these objects supports a surface polaritonic resonance (through coupling of electromagnetic excitations to either plasmon or phonon) at infrared frequencies, this resonance can be thermally excited and then couple with the adjacent object, leading to strong evanescent radiative heat transfer.[14−17] This resonant coupling can make the heat transfer occur over a quasi-monochromatic frequency distribution,[17,18] while its intensity can overcome the Stefan−Boltzmann law by several orders of magnitude. These unique features could be used to efficiently convert heat to electricity using photovoltaic (PV) cells. For this purpose, a PV cell would be placed in extreme proximity with a hot object that supports a surface resonance at a frequency that matches its bandgap excitation energy (see graphical abstract). Heat would then transfer to the PV cell mostly in the form of photons that have sufficient energy to excite electron−hole pairs and generate current. The heat-to-electricity conversion efficiency of this technology[6] could

Received: December 22, 2016
Accepted: March 13, 2017
Published: March 13, 2017

DOI: 10.1021/acsnano.6b08597
ACS Nano 2017, 11, 3001−3009

potentially outperform existing thermoelectric generators,[19] thus providing an attractive solution for solid-state electricity generation (e.g., for industrial or automotive waste heat recovery, or small scale residential generation). Despite these great promises, however, no experimental demonstration of NFTPV was yet achieved (other than for the experimental demonstration of a related "micron-gap" technology[20] based on nonresonant near-field coupling[21]).

One of the main challenges for the realization of NFTPV is its incompatibility with conventional silicon-based PV cells. At temperatures that are realistic for solid-state materials (i.e., <2000 K), Planck's spectral distribution shows negligible energy at frequencies greater than the 1.1 eV bandgap of silicon. Even by enhancing heat transfer at frequencies greater than 1.1 eV using near-field surface resonance effects, calculations show that most of the thermal radiation between any hot object and a silicon PV cell would still occur below 1.1 eV (due to conventional, blackbody-like, broadband thermal radiation). This would translate to poor NFTPV heat-to-electricity conversion efficiency since most of the thermal photons (i.e., heat) reaching the PV cell would then have insufficient energy (i.e., <1.1 eV) to excite electron−hole pairs. Thus, a PV cell with lower bandgaps (typically <0.6 eV) is desirable for NFTPV. However, performances of PV cells with bandgaps below 0.4 eV are limited by high dark current, such that the ideal bandgap range for NFTPV is typically 0.4−0.6 eV.

Most previous theoretical proposals are therefore based on low bandgap III−V semiconductors which, despite promising calculated performances, pose important challenges for experimental progress on NFTPV and for its eventual widespread application. The first complete analysis of a NFTPV generator was proposed in ref 3 where >25% efficiency and a 100 W/cm^2 power density were calculated by considering a 2000 K tungsten emitter and a GaSb PV cell separated by 10 nm. Subsequent reports calculated the potential effects of absorption distribution inside the PV cell,[4] of a backside reflector to recycle low energy photons,[9] of unwanted heating of the PV cell,[5] or of detrimental coupling of low frequency surface phonons.[11] While these reports focused on the performances of existing InGaAs- or GaSb-based PV cells, recent works provided a more generalized formalism[6,12] and estimated the performance limits of systems based on idealized emitters and semiconductor PV cells. In ref 6 a 36% conversion efficiency and a 14 W/cm^2 power density were predicted (for a 600 K emitter temperature and a 10 nm emitter-cell separation), which is significantly higher than the performances of existing thermoelectric generators (typically <10% and <5 W/cm^2 at comparable temperatures[19]). Despite these promising calculated performances, relying on III−V semiconductors is a significant limiting factor for experimental progress on NFTPV, and possibly for the eventual widespread application of the technology. The need for a specially tailored III−V cell with an unpassivated and perfectly flat front surface (required for bringing the thermal emitter to <100 nm distance from the junction), is by itself an important technical challenge that can only be achieved by few specialized laboratories.[20] Furthermore, one of the other main technical challenge of NFTPV—maintaining a sub-100 nm distance between parallel surfaces subject to large thermal gradients—was recently overcome using integrated micro-electromechanical systems (MEMS).[22−24] These solutions would be best suited for integration with silicon-based PV technology, rather than III−V, since MEMS technology is largely based on silicon and silicon compounds. Finally, cost is another fundamental consideration in energy conversion technologies, and it is not clear that a technology based on expensive III−V epitaxial crystal growth techniques would eventually become competitive. There is therefore a high probability that an eventual successful NFTPV technology based on III−V semiconductors would be limited to niche applications, much like current III−V solar cells or thermoelectric generators.

The focus of our work is therefore to develop an approach, and to provide general design rules, for NFTPV energy conversion based solely on conventional and widely available deposited thin film materials. We rely on hot carrier Schottky junctions to create silicon PV cells having excitation energies in the optimal range (ϕ_b = 0.4−0.6 eV) for NFTPV. In these junctions, carriers from the metallic film are excited above Fermi level (hence the "hot carrier" designation) by incident photons and can then overcome the Schottky barrier height (ϕ_b), thus generating electrical power (see graphical abstract). This carrier generation process generally obeys the Fowler model,[25] which typically yields insufficient quantum efficiencies (QE) for energy conversion applications. We note however that hot carrier science is currently an important topic of research,[26−32] and that several recent works[26,28−31] point to carrier generation conditions that could potentially allow the Fowler model limit to be exceeded. We show that NFTPV systems based on such junctions (i.e., with QE exceeding the Fowler limit) could—after optimization of their near-field thermal radiation spectrum—allow heat-to-electricity conversion efficiencies exceeding that of existing solid-state solutions. We provide general design rules for the spectral optimization of such a system and show that it can be achieved with well-known and widely available thin film materials (unlike previous work relying on doped graphene junctions[8]). Furthermore, we discuss how thermal radiation in the extreme near-field presents unique properties that are especially well suited for investigating recently proposed approaches[26,28−31] for high QE hot carrier junctions.

RESULTS AND DISCUSSION

System Overview. In our approach (depicted in Figure 1) the PV cell consists of a Schottky junction between a metallic layer ($TiSi_2$) and silicon. The barrier height (ϕ_b) of such Schottky junction is analogous to the semiconductor bandgap in a conventional silicon PV cell, but can take several different values as a function of the materials used to create the junction.[33] For example, $TiSi_2$—a commonly used and well characterized compound in integrated electronic circuits—forms a ϕ_b = 0.45 eV barrier height with p-type silicon,[34] which is within the optimal 0.4−0.6 eV range for NFTPV. Its optical properties, as will be discussed in the next section, are also ideal to maximize evanescent coupling with the infrared surface resonance of the hot plasmonic light emitter. This plasmonic emitter, made of indium-tin-oxide (ITO), supports a surface resonance at a frequency $\omega_{res} \sim 0.6$ eV slightly larger than ϕ_b in order to maximize the flux of photons of energies larger than the barrier height (the design of this emitter will also be discussed in greater detail in the next section). These photons, when coupling from the emitter surface to the junction metallic ($TiSi_2$) layer, excite charge carriers over the ϕ_b junction barrier height, thus creating electron−hole pairs that are separated (see Figure 1b) and converted to useful electrical power by the junction.

DOI: 10.1021/acsnano.6b08597
ACS Nano 2017, 11, 3001−3009

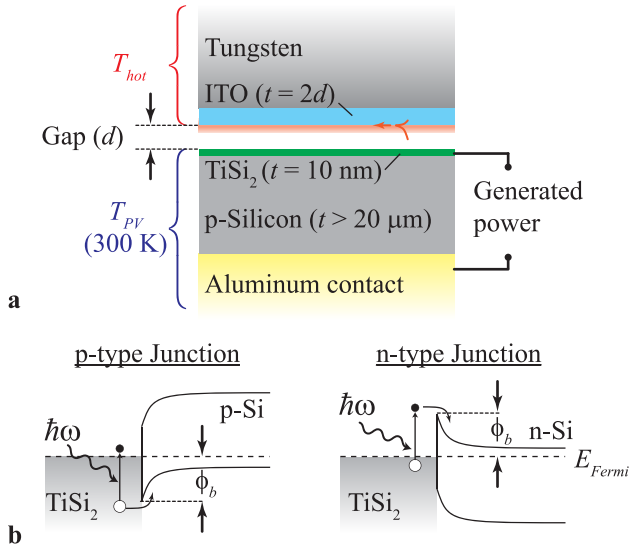

Figure 1. (a) Cross section of the hot carrier-based near-field thermophotovoltaic generator considered in this work. The indium-tin-oxide (ITO) layer supports a thermally excited surface resonance at frequency (0.61 eV) slightly superior to the barrier height (ϕ_b) of the $TiSi_2$−silicon Schottky junction (0.45 eV). At near-field distances, the ITO surface resonance couples with the silicide layer and excites charge carriers above the junction barrier height, thus generating photocurrent. The thickness of the ITO film is tailored as a function of the separation to maximize the efficiency. The tungsten layer acts essentially as a mechanical support. The aluminum layer acts both as the junction back electrode and as a back mirror that recycles low energy photons back to the emitter. (b) Band diagram of the hot carrier generation process on either p-type (left) or n-type (right) semiconductor.

Our main goal is to maximize the overall heat-to-electricity conversion efficiency (η_{tot}) of the system, which depends (1) on the Q(ω) radiation spectrum between the two objects, (2) on the junction quantum efficiency (QE), and (3) on the efficiency η_{jct} with which the junction converts photogenerated charge carrier pairs to electrical power:

$$\eta_{tot} = \eta_{jct} \times \int_{\phi_b/\hbar}^{\infty} \frac{\phi_b}{\hbar\omega}\cdot QE(\omega)\cdot Q(\omega)\, d\omega / \int_0^{\infty} Q(\omega)\, d\omega \quad (1)$$

Since controlling the QE of hot carrier devices is currently a rapidly evolving field of research,[26,28−31] we focus our analysis here on how the electromagnetic design can impact the efficiency of the system. Therefore, we will first set a frequency independent QE at $\hbar\omega > \phi_b$. We will later review, in the context of NFTPV, different approaches for achieving high QE hot carrier generation. In this case, we can take QE out of the integral in eq 1 and break down η_{tot} in separate contributions that depend only on the PV cell efficiency (i.e, $\eta_{jct} \times$ QE) and on the $Q(\omega)$ radiation spectrum between the hot emitter and the cell (i.e., the integrals in eq 1, which we now denote as the η_{spec} spectral efficiency):

$$\eta_{tot} = \eta_{jct} \times QE \times \eta_{spec} \quad (2)$$

The η_{spec} spectral efficiency quantifies the fraction of radiated photons having higher energy than the ϕ_b junction barrier, and also accounts for the ($\hbar\omega - \phi_b$) energy loss that occurs when a photon with $\hbar\omega > \phi_b$ excites a charge carrier pair. It therefore depends only on ϕ_b and on the $Q(\omega)$ radiation spectrum between the emitter and the PV cell, and it is optimized by making sure that most of the radiation occurs above, but relatively close to, the excitation energy ϕ_b (e.g., η_{spec} = 100% would happen for perfectly monochromatic illumination exactly at $\omega = \phi_b/\hbar$). While ϕ_b strongly influences η_{spec}, it must also be taken into consideration for the optimization of η_{jct}. As in conventional solar cells, η_{jct} depends on the junction current−voltage (I−V) response and is optimized by increasing ϕ_b. Higher ϕ_b minimizes the reverse bias (i.e., "dark") current, which in turn maximizes the junction open voltage ($V_{oc} \leq \phi_b$) and η_{jct}. In the following sections, we will first maximize η_{spec} by optimizing the radiation spectrum between the thermal emitter and the PV cell. We will then calculate the overall efficiency (η_{tot}) by calculating the junction I−V response under our previously optimized near-field thermal radiation condition.

Spectral Efficiency. We maximize the η_{spec} spectral efficiency by calculating (using the formalism described in ref 35) the near-field heat transfer spectrum ($Q(\omega)$) between two isotropic one-dimensional multilayer stacks. $Q(\omega)$ is the sum of the spectra of propagating (Q_{prop}) and evanescent waves (Q_{evan}), which are given by

$$Q_{prop}(\omega) = \frac{\Theta(\omega, T_{hot}) - \Theta(\omega, T_{PV})}{4\pi^2} \cdot \sum_{TE,TM} \int_0^{k_v} \frac{(1 - |R_{emit}^{TE,TM}|^2)(1 - |R_{PV}^{TE,TM}|^2)}{|1 - R_{emit}^{TE,TM} R_{PV}^{TE,TM} e^{2ik_z d}|^2} k_\rho dk_\rho \quad (3)$$

$$Q_{evan}(\omega) = \frac{\Theta(\omega, T_{hot}) - \Theta(\omega, T_{PV})}{4\pi^2} \cdot \sum_{TE,TM} \int_{k_v}^{\infty} \frac{\mathrm{Im}(R_{emit}^{TE,TM})\mathrm{Im}(R_{PV}^{TE,TM})}{|1 - R_{emit}^{TE,TM} R_{PV}^{TE,TM} e^{2ik_z d}|^2} e^{2id\mathrm{Im}(k_z)} k_\rho dk_\rho \quad (4)$$

where Θ is the Planck mean oscillator energy:

$$\Theta(\omega, T) = \frac{\hbar\omega}{e^{\hbar\omega/k_b T} - 1} \quad (5)$$

T_{hot} is the emitter temperature, T_{PV} is the PV cell temperature (set to 293 K), $k_v = \omega/c$ is the vacuum wavevector, k_ρ is the wavevector parallel to the multilayer stacks, $k_z = \sqrt{k_v^2 - k_\rho^2}$ is the perpendicular wavevector in vacuum, and d is the emitter-cell separation. R_{emit} and R_{PV} are the amplitude reflection coefficients of the individual multilayer stacks formed by the emitter and the PV cell, respectively. These coefficients can be calculated, using conventional optical multilayer formalism, as a function of polarization (TE or TM), k_ρ, and of the $\varepsilon(\omega)$ layer permittivities. Special care must however be given to numerical instability when dealing with high k_ρ evanescent waves and highly absorbing materials (see numerically stable solutions of R_{EMIT} and R_{PV} in Methods). Throughout this work, we always calculate the heat transfer for both polarization and for both propagating and evanescent waves. We note however that at the very small distances of interest for our work, the heat transfer is dominated by TM evanescent waves.

We first note that optimizing η_{spec} is especially challenging for hot carrier NFTPV since, unlike in conventional PV cells, the junction does not benefit from a strong change of its optical absorption at the junction excitation energy (i.e., at $\omega = \phi_b/\hbar$). In NFTPV systems based on conventional semiconductor junctions, the semiconductor material selectively absorbs light only at frequencies greater than the material bandgap. This

DOI: 10.1021/acsnano.6b08597
ACS Nano 2017, 11, 3001−3009

selective absorption, which results from the intrinsic property of the semiconductor itself, makes the choice of the thermal emitter material much less critical. In ref 3, for example, a simple tungsten emitter—which does not support a surface resonance at a frequency matching the bandgap of GaSb—is found to allow similar efficiency and power density as an ideal quasi-monochromatic surface resonant emitter (at 2000 K temperature and $d \geq 10$ nm). In refs 9 and 11 tungsten is also found to be an appropriate emitter for lower temperatures as long as a back mirror on the PV cell is used to recycle low frequency radiation back to the emitter. In hot carrier Schottky cells, however, the layer forming the junction with the semiconductor is metallic and can therefore absorb light very efficiently at all frequencies (including those below the junction barrier height). An emitter supporting a surface resonance at an frequency matching ϕ_b is therefore crucial in order to enhance the emitter surface density of states,[36] and hence the radiated power, at frequencies greater than the junction barrier height.

We use ITO as the emitter material as it supports a surface resonance in a frequency range ($\omega_{res} \sim 0.4-0.9$ eV) that matches the ideal barrier height ($\phi_b = 0.4-0.6$ eV) for NFTPV. For material permittivities ($\varepsilon(\omega)$) described by a free electron Drude model:

$$\varepsilon(\omega) = \varepsilon_\infty\left(1 + \frac{\omega_p^2}{\omega^2 + i\omega\Gamma}\right) \tag{6}$$

surface resonance at the material−vacuum interface occurs for $\mathrm{Re}(\varepsilon) = -1$,[36] and ω_{res} is given by

$$\omega_{res} = \sqrt{\frac{\varepsilon_\infty}{\varepsilon_\infty + 1}\omega_p^2 + \Gamma^2} \approx \sqrt{\frac{\varepsilon_\infty}{\varepsilon_\infty + 1}}\omega_p \tag{7}$$

From eq 7, we note that we can obtain ω_{res} at frequencies matching ϕ_b using indium tin oxide (ITO), which typically has $\varepsilon_\infty = 4$, $\omega_p \sim 0.4-0.9$, and $\Gamma \sim 0.1-0.15$ eV[6,37] as the emitter. Other transparent conductive oxides,[37−39] or titanium nitride-based metamaterials,[40] would also work but we choose to consider ITO here for its wide availability, the ease with which ω_p can be adjusted by controlling the amount of oxygen during deposition, and its proven high temperature stability up to 1400 °C.[41] We also note that, although transparent conductive oxides suffer from reduced charge carrier mobility at high temperatures ($\mu \propto 1/T$),[42] this reduction can be expected to have a limited impact on the plasmon damping rate (Γ). Extrapolating for $T > 500$ K the experimental data presented in ref 42 yields < 50% temperature induced variations of μ (and hence of $\Gamma \propto \mu$) for the temperatures of interest for our work. This is within the range of typical μ variations resulting from other factors such as film annealing and deposition conditions.[43]

For the Schottky junction metallic film, we use a metal silicide alloy (i.e., $TiSi_2$), rather than a pure metal, in order to maximize optical coupling with the ITO resonance and maximize η_{spec}. Near-field radiative heat transfer is maximum when both materials involved support surface resonances that overlap in frequency.[36] The metallic film forming the junction therefore has an important influence on the thermal radiation spectrum and must be chosen to have a surface resonance as close as possible from that of ITO. Several pure metals films, when deposited on silicon, will form Schottky junctions with barriers in the optimal $\phi_b = 0.4-0.6$ eV range for NFTPV. Metals however have very high ω_p (5−15 eV[44]) due to their very high density N_e of free electrons ($\omega_p \propto \sqrt{N_e}$) and therefore offer poor optical coupling with the ITO resonance. Metal silicides typically have lower N_e and ω_p (2−5 eV[45]) and therefore allow better coupling. We iteratively calculate the heat transfer spectrum between ITO and several different metal silicides from their permittivities available in the SOPRA material database[46] (we do not use a simple Drude model, unlike for ITO, since such model is inaccurate for silicides for $\omega < 1$ eV due to non-negligible interband absorption[47]). We find that $TiSi_2$ yields the best coupling with ITO at $\omega \sim 0.4-0.8$ eV, while forming an ideal $\phi_b = 0.45$ eV barrier height with p-type silicon.[34] We subsequently compare the $TiSi_2$ permittivity found in the online database[46] with published data[45,48] in order to ascertain its accuracy. We find as a general trend that silicides with high electrical conductivity and low metal molecular fraction (e.g., 33% for $TiSi_2$) yield the best coupling with the ITO emitter surface resonance and the lowest unwanted heat transfer at frequencies below ϕ_b.

Having chosen both the emitter (ITO) and junction ($TiSi_2$) materials we finally fine-tune η_{spec} by investigating the effect of other parameters such as film thicknesses, the exact ITO permittivity, and the presence of other films in the emitter and PV cell multilayer stacks. We optimize the plasmon frequency of ITO (as can be done experimentally within the $\omega_p \sim 0.4-0.9$ eV frequency range by controlling the amount of oxygen during deposition[37]) and find $\omega_p = 0.685$ eV as the optimal value for maximizing η_{spec} (with $\Gamma = 0.12$ eV and $\varepsilon_\infty = 4$ fixed from literature values[6,37]). We find that the effect of the silicon substrate thickness is negligible for thickness greater than 20 μm, and that considering a metal back electrode (e.g., aluminum in our case, see Figure 1a) yields a small but noticeable increase (~2%) of efficiency by recycling some of the lower frequency radiation back to the emitter. The $TiSi_2$ film is set to be thin (10 nm) to allow hot carriers excited at the silicide-vacuum surface to reach the silicide−silicon interface before decaying.[26] We observe that a thermal emitter consisting of a thin ITO film yields higher η_{spec} than a semi-infinite ITO bulk emitter. This is illustrated in Figure 2a, where a thin ITO emitter deposited on tungsten radiates less unwanted energy at frequencies below ϕ_b than a bulk ITO emitter (due to lower effective absorption/emission length in a thin film compare to a bulk). We consider tungsten as the mechanical support for the ITO film for its high temperature stability, but other materials such as silicon would yield comparable performances. As observed also in ref 35, the ideal ITO film thickness in this case is not constant but depends on the gap (d) between the objects. This dependency is calculated in Figure 2b), from which we note that fixing the ITO thickness to $t \sim 2d$ yields η_{spec} close to optimal values for the distances of greater interest for our work (i.e., $d = 10-40$ nm).

Using this fully optimized system, we achieve over 50% spectral efficiency for gaps in the 10−30 nm range and temperatures above 900 K (see Figure 3). Smaller distances between the emitter and the PV cell yield better evanescent coupling between the ITO surface resonance and the PV cell, thus increasing both the spectral efficiency and the heat transfer power. Higher temperatures also increase the spectral efficiency as the blackbody envelope shifts to higher frequencies and therefore yields a higher fraction of useful photons (see Figure 3a). In comparison, using tungsten only as the near-field emitter (as for NFTPV based on semiconductor PV cells[3,9,11]), would yield $\eta_{spec} < 6\%$ for a 10 nm gap at 900 K (see Figure 2). We note also that the total effective power (total power × η_{spec}) at 10 nm distance is 100× higher than the maximum achievable

DOI: 10.1021/acsnano.6b08597
ACS Nano 2017, 11, 3001−3009

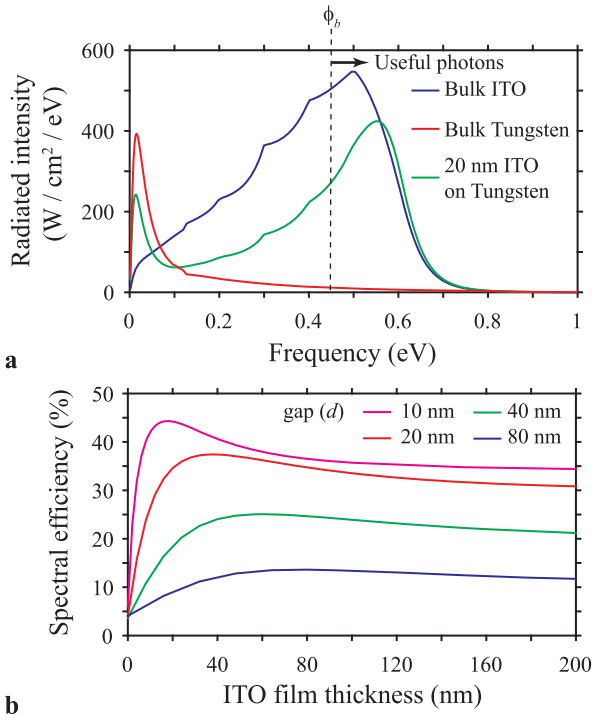

Figure 2. (a) Heat transfer spectrum between the hot carrier PV cell and various thermal emitters at T = 900 K and d = 10 nm. Using a 20 nm thick ITO film deposited on tungsten as the emitter allow a high flow of useful photons, but with a greatly reduced flow of unwanted low energy photons ($\hbar\omega < \phi_b$) compared to a bulk ITO emitter. (b) Spectral efficiency as a function of the ITO film thickness, for various emitter-cell gap. The ITO film thickness that maximizes the spectral efficiency increases with the gap.

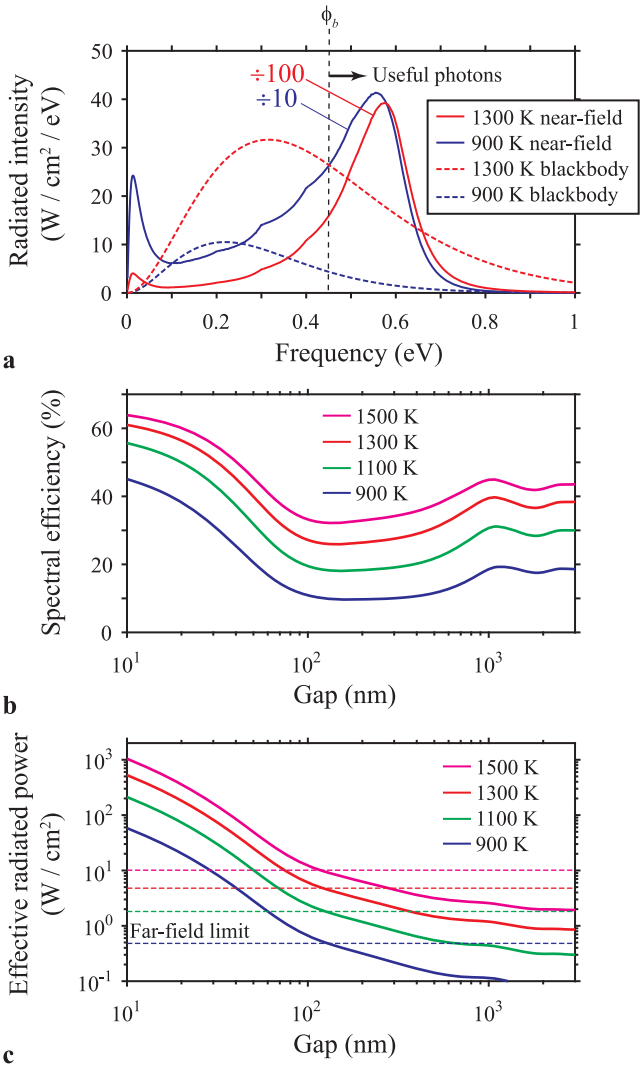

Figure 3. (a) Optimized radiation spectra at 10 nm separation between the emitter and the PV cell and comparison with blackbody spectra at the same temperatures. Only photons with energies higher than the ϕ_b barrier height can generate carriers in the Schottky cell. (b) Spectral efficiency for different emitter temperatures as a function of the distance with the PV cell. At distances < 100 nm, spectral efficiency increases with smaller gaps due to better coupling of the ITO surface resonance with the PV cell. (b) Effective radiated power (i.e., total power × spectral efficiency) between the emitter and the cell. Distances < 100 nm allow significantly higher intensities than achievable using far-field emitters (i.e., blackbody).

using a far-field blackbody (see Figure 3c). Interestingly, this 100× enhancement is stronger than obtained by considering III−V PV cells since our metal silicide acts as a stronger light absorber than a semiconductor (in ref 3 for example, 35× enhancement is achieved using an idealized emitter and a GaSb cell). This stronger enhancement could eventually relax the distance requirement between the emitter and the PV cell compared to system based on III−V cells.

Overall Efficiency. Having optimized η_{spec} (and considering, as discussed earlier, QE = 100% for $\hbar\omega > \phi_b$), we can finally calculate the overall efficiency (η_{tot}) by calculating the junction current voltage response (i.e., η_{jct} in eq 2). As for solar cells, there is no simple closed form expression for η_{jct}, but the total efficiency can easily be calculated numerically from the current density (j_{cell}) in the junction:

$$j_{cell}(V) = j_{sc} - j_{sat}\left(e^{qV/k_B T_{PV}} - 1\right) \tag{8}$$

where V is the voltage, k_B is the Boltzmann constant, j_{sat} is the reverse bias saturation (i.e., "dark") current, and j_{sc} is the short circuit current. The reverse saturation current must be kept as small as possible in order to maximize efficiency and is given by

$$j_{sat} = A^* \cdot T_{PV}^2 \, e^{-\phi_b/k_B T_{PV}} \tag{9}$$

where A^* is the effective Richardson constant (32 A/(cm^2/K^2) for p-type silicon[49]). While we have set T_{PV} = 293 K here for simplicity, we note that eq 9 could be used for calculating the effect of spurious heating of the junction under various heat extraction conditions.[5] The short circuit current results from photogenerated carriers in the junction and is given by

$$j_{sc} = q \int_{\phi_b/\hbar}^{\infty} \frac{Q(\omega)}{\hbar\omega} \cdot QE(\omega)\, d\omega \tag{10}$$

where q is the electron charge. Since we consider QE as constant (for $\hbar\omega > \phi_b$) eq 10 can conveniently be rewritten as a function of the total radiated power between the emitter and cell (P_{tot}):

$$j_{sc} = \frac{q}{\phi_b} QE \cdot P_{tot} \cdot \eta_{spec} \tag{11}$$

This notation clearly outlines the importance of optimizing η_{spec} to maximize the output current of the junction. Using eqs 8 to 11, we can calculate the electrical power output of the

DOI: 10.1021/acsnano.6b08597
ACS Nano 2017, 11, 3001−3009

junction (P_{gen}) by numerically finding the junction optimal operation voltage:

$$P_{gen} = \max(V \cdot j_{cell}(V)) \quad (12)$$

from which we finally obtain the overall efficiency:

$$\eta_{tot} = P_{gen}/P_{tot} \quad (13)$$

In the following results, we normalize η_{tot} by QE in order to emphasize the strong influence of the QE on the overall efficiency. This normalized efficiency can also be used to approximate η_{tot} for any QE ≠ 100% value. This procedure should however be seen as an upper bound approximation of η_{tot} (unless QE = 100%). The rigorously exact value of η_{tot} for QE ≠ 100% would be obtained by re-evaluating the numerical solution of eq 12 in order to account for the effect of charge density on the junction efficiency (i.e., higher charge density is beneficial to the junction efficiency as also occurs, for example, in solar cells under concentrated illumination). We find however that this upper bound approximation is accurate within 10% error for QE in the 50%−100% range.

When considering an idealized 100% QE for the Schottky junction, our system reached overall heat-to-electricity conversion efficiencies (η_{tot}) in the 10−30% range, and power densities in the 10−500 W/cm^2 range (see Figure 4). This efficiency is significantly higher than the experimentally reported performances of thermoelectric generators (<10%[19]) and could therefore provide a competitive solution for high efficiency solid-state conversion of heat to electricity. We also note that our efficiency is comparable to the predictions of NFTPV based on state-of-the-art III−V *pn* junction PV cells,[3]

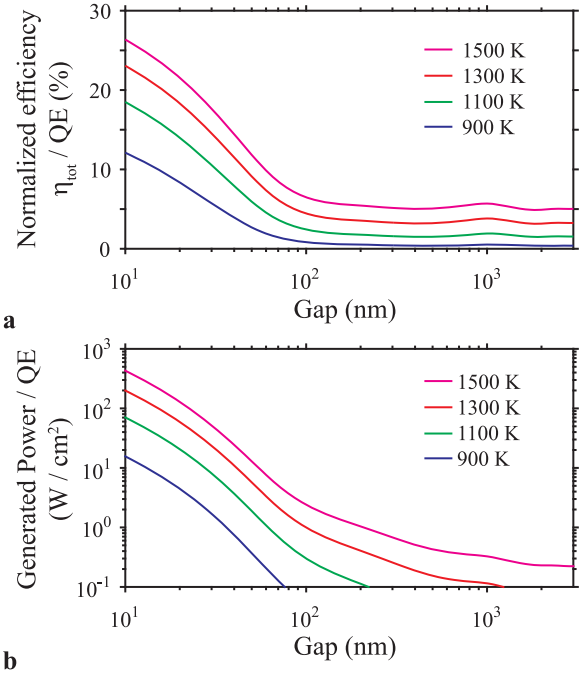

Figure 4. (a) Total conversion efficiency (η_{tot}) (normalized by the quantum efficiency) of hot carrier NFTPV at different temperatures. With an ideal QE = 100%, the total efficiency is comparable to NFTPV based on epitaxial III−V semiconductors and is higher than experimental reports on thermoelectric generators.[19] (b) Generated power per module unit area, also normalized by the PV cell quantum efficiency.

despite the fact that we rely on a Schottky junction, in which dark current is higher than in typical *pn* junctions. In our configuration, however, the detrimental effect of high dark current is compensated by the beneficial effect of higher radiation intensity (caused by stronger absorption in the metal silicide layer). As discussed above, this higher intensity improves the efficiency as it also does, for example, when solar radiation is concentrated on a solar cell.

While these results were obtained for the specific case of a ϕ_b = 0.45 eV barrier height, other materials with slightly different ϕ_b values could potentially yield similar or better performances. To quantify the range of optimal ϕ_b values for future research on hot carrier NFTPV, we simulate η_{tot} as a function of ϕ_b at various emitter temperatures. For this simulation, we approximate the radiation spectrum as a blackbody distribution enhanced by a factor of 100 at $\omega > \phi_b/\hbar$, and by a factor of 20 at $\omega < \phi_b/\hbar$. Such approximation matches very well the spectral efficiencies and the effective radiated powers obtained in Figure 3 (for d = 10 nm). Our simulation (Figure 5) clearly shows an

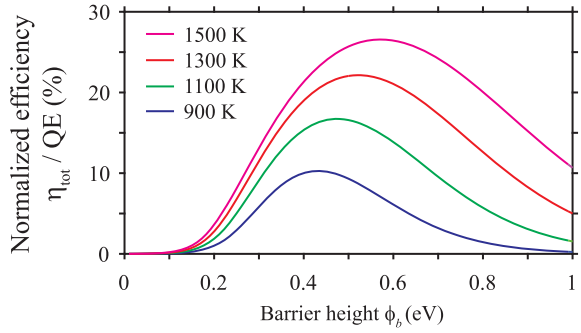

Figure 5. Ideal Schottky barrier height for different emitter temperatures. For this calculation, the heat transfer spectrum is approximated as a blackbody multiplied by a factor of 100 at frequencies above the barrier height, and by a factor of 20 below the barrier height. The ideal barrier height is in the 0.4−0.6 eV range, below which the dark current (eq 9) degrades the photovoltaic efficiency, and above which the fraction of radiated power above the barrier height is too low (i.e., low η_{spec}).

optimal range for ϕ_b between approximately 0.4 and 0.6 eV, depending on the emitter temperature. Barrier heights lower than 0.4 eV lead to very high dark current values (see eq 9) that are detrimental to the η_{jct} junction efficiency, while increasing the barrier height beyond 0.6 eV leads to a higher fraction of radiation below the barrier height (i.e., lower η_{spec} spectral efficiency). Interestingly, the optimal ϕ_b value increases with temperature since the blackbody envelope shifts to higher frequencies, thus allowing high η_{spec} spectral efficiencies for higher ϕ_b values. This behavior should be accounted for when designing NFTPV systems for a specific operation temperature.

Quantum Efficiency. Several approaches[26,28−31] are currently investigated for increasing the QE of hot carrier devices beyond conventional Fowler model predictions, and (as for several other applications of hot carriers) the feasibility of our proposed NFTPV system will ultimately depend on the outcome of these researches. We argue here that the particularities of metal silicide junctions—and of thermal radiation in the extreme near-field—are especially well aligned with several of these recently proposed approaches. The conventional Fowler model[25,27] for hot carrier emission in Schottky junctions considers a free electron gas approximation

DOI: 10.1021/acsnano.6b08597
ACS Nano 2017, 11, 3001−3009

for the carrier density of states (DOS) in the junction metallic layers, which leads to QEs that are fundamentally too low for NFTPV. In this model, the DOS in the metallic layer is a continuum, such that carriers can be excited from various energy depths below the Fermi level (e.g., see n-type junction energy diagram in Figure 1b). This depth adds to the ϕ_b barrier that they must overcome to reach the semiconductor,[26] thus greatly decreasing the QE. Within this framework, even in the best case scenario where the film is very thin (allowing multiple interaction of an excited electron with the junction interface) and nanostructured (to relax requirements on the excited electron propagation direction[26]), QE is given by[27]

$$\mathrm{QE}(\omega) = 1 - \frac{\phi_b}{\hbar\omega} \tag{14}$$

which is insufficient for hot carrier NFTPV to reach competitive performances. For example, at the 0.55 eV emission peak in Figure 3a, QE would only be 20%, such that η_{tot} in Figure 4 would be <4%.

Engineering the metallic layer DOS to differ from that of a free electron gas is therefore one of the main approaches for enhancing QE beyond the Fowler model limit, and we find that this approach is highly compatible with silicide based NFTPV. In this approach, the silicide DOS in Figure 1b would be engineered to no longer be the continuum resulting from a free electron model, but to show a sharp maximum just below the Fermi level. More carriers would consequently be excited from an initial energy that is close from the Fermi level and would hence end up with enough energy to overcome the ϕ_b barrier height, potentially leading to QEs close to 100%.[26] A first method for such DOS engineering consists of directly identifying materials that present the desired discontinuities in their DOS, or of creating such material by investigating different alloys.[26] This method has not been investigated in much detail to date, and we point out that the great variety of metals from which silicides can controllably be grown[50,51] on silicon, simply by annealing of thin metal films, could provide the ideal platform to do so. The second method for engineering the DOS has attracted more attention[28,29] and consists of discretizing the DOS in the metallic film by reducing its dimension (instead of engineering the material itself[26]). Again, we find that silicide-based NFTPV offers interesting opportunities for pursuing this direction. We first note that this method is especially well suited for a system—such as ours—based on evanescent radiation. For systems based on propagating waves (e.g., solar cells), reduced dimensions impose a performance trade-off[28] (i.e., a large metal absorber allows high absorption, while small dimensions allow higher QE). On the contrary, evanescent radiation naturally allows strong absorption in very small dimensions (e.g., the 10 nm $TiSi_2$ layer in Figure 1a) and hence does not suffer from the same trade-off. We note also that silicide formation by thermal annealing of metal films can create high quality continuous layers as thin as 2 nm,[52] and that the silicide film in our junction could easily be patterned to provide carrier confinement in the transverse dimension. Moreover, we note that forming metal silicides from metal thin films by thermal annealing consumes a fraction of the underlying silicon substrate. As a result, nanostructuring a metal layer before annealing would create silicide nanostructures that are partially embedded in the silicon substrate. Such embedding was experimentally proven to enhance the hot electron emission process[53] and could be advantageous compared to other configurations. We finally note that for any of these DOS engineering approaches, near-field thermal radiation models[4] can allow calculation of the exact depth at which charge carriers are excited inside the metal film, which could prove useful for a more detailed investigation of electronic transport inside the junction.

Rather than engineering the whole metallic layer DOS, other works show[30,31] that hot carrier quantum efficiency could be enhanced by favoring specific interband transitions in the metallic layer, which we find is also a promising approach for NFTPV. These works show that, even in noble metals, a simple free electron gas model is not always appropriate for describing hot carrier generation, and that the complete material band structure should be considered. The authors consequently point out that matching the momentum of plasmonic surface excitation with the momentum change associated with a given interband transition could be used to favor a specific transition that maximizes the hot carrier generation process.[31] One of the main challenges in achieving this approach is the typically very large momentum of charge carriers in solids compared to the momentum of photons.[26] In this context, our approach could be advantageous since near-field thermal radiation is mediated by photons having much higher momentum ($\hbar k$) than free space radiation (i.e., $k_\rho > k_v$ in eq 4). For example, for the 1300 K heat transfer spectrum in Figure 3a, 75% of the heat transfer at the 0.55 eV peak frequency results from photons having k_ρ in the $10k_v$–$35k_v$ range. Interestingly, the upper limit for this range is tunable[35] as it depends on the distance d, as $k_\rho \sim 1/d$. We finally note that various interband transitions in the silicide layer could be also investigated simply by growing silicides on silicon substrate having different crystallographic orientations.[54]

CONCLUSION

We provided general design rules for hot carrier-based NFTPV and demonstrated the great potential of this technology for solid-state electricity generation. Our work shows that hot carrier-based NFTPV could allow conversion of heat to electrical power with greater efficiencies than current thermoelectric generators. Such technology could find applications for waste heat recovery in vehicles and industries, or for small scale (e.g., residential) electricity generation from alternative energy sources. By replacing III–V semiconductors with simple and widely available thin films, our work also provides a path that could finally allow experimental progress on NFTPV, more than 10 years after the original theoretical proposals.[1−3] The success of our approach, as for several other applications of hot carriers, will ultimately depend on the advance of researches on enhancing the QE of hot carrier devices beyond conventional Fowler model predictions. We have reviewed recently proposed approaches for reaching that goal and discussed how the properties of thermal radiation in the extreme near-field provide interesting research opportunities along those directions. We also pointed out how the properties of metal silicides—on which we relied here mostly for their ability to optically couple with near-infrared surface waves—are well aligned with these QE enhancement approaches. We therefore expect our work to be of interest for researchers working both on NFTPV and on hot carrier science, and hence to create bridges between these two fields.

METHODS

Numerical Calculations. Radiative heat transfer calculations are carried by numerically evaluating the integral in eqs 3 and 4. For evanescent waves (eq 4), the integral upper bound is set to $k_\rho = 10/d$.

DOI: 10.1021/acsnano.6b08597
ACS Nano 2017, 11, 3001−3009

The amplitude reflection coefficients of the multilayer stacks formed by the emitter (R_{EMIT}) and the PV cell (R_{PV}) are calculated as a function of parallel wavevector k_ρ and of the layers refractive indices (n) using a numerically stable optical multilayer calculation algorithm. For a multilayer stack comprising N interfaces (numbered from 1 to N starting at the incidence interface) and $N + 1$ isotropic materials (numbered from 0 to N), we denote medium 0 as the incidence medium (vacuum in our case) and N as output medium (in our case either aluminum for R_{PV} or tungsten for R_{EMIT}, see Figure 1). The effective amplitude reflection coefficient at the incidence interface (R_1) is calculated incrementally starting at the last (Nth) interface (i.e., $j = N - 1$) using

$$R_j = \frac{r_j + R_{j+1}\, e^{2i\sqrt{k_j^2 - k_\rho^2}\, t_j}}{1 + r_j R_{j+1}\, e^{2i\sqrt{k_j^2 - k_\rho^2}\, t_j}} \tag{15}$$

In eq 15, t_j it the thickness of the jth layer, r_j is the Fresnel reflection coefficient of the jth interface, and $k_j = 2\pi/n_j$ is the wavevector in the jth medium. The interfacial Fresnel coefficients r_j are given by eqs 16 and 17, respectively for TM and TE polarization:

$$r_j^{TE} = \frac{\sqrt{k_j^2 - k_\rho^2} - \sqrt{k_{j+1}^2 - k_\rho^2}}{\sqrt{k_j^2 - k_\rho^2} + \sqrt{k_{j+1}^2 - k_\rho^2}} \tag{16}$$

$$r_j^{TM} = \frac{\frac{k_{j+1}}{k_j}\sqrt{k_j^2 - k_\rho^2} - \frac{k_j}{k_{j+1}}\sqrt{k_{j+1}^2 - k_\rho^2}}{\frac{k_{j+1}}{k_j}\sqrt{k_j^2 - k_\rho^2} + \frac{k_j}{k_{j+1}}\sqrt{k_{j+1}^2 - k_\rho^2}} \tag{17}$$

Equation 15 is evaluated incrementally starting at the last (Nth) interface, all the way up to the incidence interface to obtain R_1 (which corresponds to either R_{EMIT} or R_{PV}). The initial condition for this incremental calculation is $R_N = r_N$. For these calculations, the refractive index of silicon is set to a constant $n = 3.45$ value, the refractive index of aluminum is approximated by a Drude model with parameters taken from ref 55, and the refractive index of tungsten is taken from ref 56 and then extrapolated at long wavelengths using a Drude model fit ($\omega_p = 5.7$ eV, $\Gamma = 0.55$ eV). The refractive indices of ITO and $TiSi_2$ are discussed in the main text (see spectral efficiency section).

AUTHOR INFORMATION

Corresponding Author

*E-mail: ml3745@columbia.edu.

ORCID

Raphael St-Gelais: 0000-0003-0866-287X

Present Address

#R.S.-G.: Department of Physics, McGill University, Montreal, Québec H3A 2T8, Canada.

Notes

The authors declare no competing financial interest.

ACKNOWLEDGMENTS

This work was funded by the Advanced Research Projects Agency-Energy (ARPA-E), IDEAS program (project title: Demonstration of Near-Field Thermophotovoltaic (TPV) Energy Generation).

REFERENCES

(1) Whale, M. D.; Cravalho, E. G. Modeling and Performance of Microscale Thermophotovoltaic Energy Conversion Devices. *IEEE Trans. Energy Convers.* **2002**, *17*, 130−142.

(2) Narayanaswamy, A.; Chen, G. Surface Modes for Near Field Thermophotovoltaics. *Appl. Phys. Lett.* **2003**, *82*, 3544−3546.

(3) Laroche, M.; Carminati, R.; Greffet, J.-J. Near-Field Thermophotovoltaic Energy Conversion. *J. Appl. Phys.* **2006**, *100*, 063704.

(4) Park, K.; Basu, S.; King, W. P.; Zhang, Z. M. Performance Analysis of Near-Field Thermophotovoltaic Devices Considering Absorption Distribution. *J. Quant. Spectrosc. Radiat. Transfer* **2008**, *109*, 305−316.

(5) Francoeur, M.; Vaillon, R.; Pinar Mengüç, M. Thermal Impacts on the Performance of Nanoscale-Gap Thermophotovoltaic Power Generators. *IEEE Trans. Energy Convers.* **2011**, *26*, 686−698.

(6) Ilic, O.; Jablan, M.; Joannopoulos, J. D.; Celanovic, I.; Soljačić, M. Overcoming the Black Body Limit in Plasmonic and Graphene Near-Field Thermophotovoltaic Systems. *Opt. Express* **2012**, *20*, A366−A384.

(7) Messina, R.; Ben-Abdallah, P. Graphene-Based Photovoltaic Cells for Near-Field Thermal Energy Conversion. *Sci. Rep.* **2013**, *3*, 1383.

(8) Svetovoy, V. B.; Palasantzas, G. Graphene-on-Silicon Near-Field Thermophotovoltaic Cell. *Phys. Rev. Appl.* **2014**, *2*, 034006.

(9) Bright, T. J.; Wang, L. P.; Zhang, Z. M. Performance of Near-Field Thermophotovoltaic Cells Enhanced with a Backside Reflector. *J. Heat Transfer* **2014**, *136*, 062701−062701.

(10) Chang, J.-Y.; Yang, Y.; Wang, L. Tungsten Nanowire Based Hyperbolic Metamaterial Emitters for Near-Field Thermophotovoltaic Applications. *Int. J. Heat Mass Transfer* **2015**, *87*, 237−247.

(11) Chen, K.; Santhanam, P.; Fan, S. Suppressing Sub-Bandgap Phonon-Polariton Heat Transfer in Near-Field Thermophotovoltaic Devices for Waste Heat Recovery. *Appl. Phys. Lett.* **2015**, *107*, 091106.

(12) Molesky, S.; Jacob, Z. Ideal Near-Field Thermophotovoltaic Cells. *Phys. Rev. B: Condens. Matter Mater. Phys.* **2015**, *91*, 205435.

(13) Mirmoosa, M. S.; Simovski, C. Micron-Gap Thermophotovoltaic Systems Enhanced by Nanowires. *Phot. Nano. Fundam. Appl.* **2015**, *13*, 20−30.

(14) Polder, D.; Van Hove, M. Theory of Radiative Heat Transfer between Closely Spaced Bodies. *Phys. Rev. B* **1971**, *4*, 3303−3314.

(15) Shchegrov, A. V.; Joulain, K.; Carminati, R.; Greffet, J.-J. Near-Field Spectral Effects Due to Electromagnetic Surface Excitations. *Phys. Rev. Lett.* **2000**, *85*, 1548−1551.

(16) Mulet, J.-P.; Joulain, K.; Carminati, R.; Greffet, J.-J. Enhance Radiative Heat Transfer at Nanometric Distances. *Microscale Thermophys. Eng.* **2002**, *6*, 209−222.

(17) Jones, A. C.; Raschke, M. B. Thermal Infrared Near-Field Spectroscopy. *Nano Lett.* **2012**, *12*, 1475−1481.

(18) Babuty, A.; Joulain, K.; Chapuis, P.-O.; Greffet, J.-J.; De Wilde, Y. Blackbody Spectrum Revisited in the Near Field. *Phys. Rev. Lett.* **2013**, *110*, 146103.

(19) Liu, W.; Jie, Q.; Kim, H. S.; Ren, Z. Current Progress and Future Challenges in Thermoelectric Power Generation: From Materials to Devices. *Acta Mater.* **2015**, *87*, 357−376.

(20) DiMatteo, R. S.; Greiff, P.; Finberg, S. L.; Young-Waithe, K. A.; Choy, H. K. H.; Masaki, M. M.; Fonstad, C. G. Enhanced Photogeneration of Carriers in a Semiconductor *via* Coupling across a Nonisothermal Nanoscale Vacuum Gap. *Appl. Phys. Lett.* **2001**, *79*, 1894−1896.

(21) Pan, J. L.; Choy, H. K. H.; Fonstad, C., Jr. Very Large Radiative Transfer over Small Distances from a Black Body for Thermophotovoltaic Applications. *IEEE Trans. Electron Devices* **2000**, *47*, 241−249.

(22) St-Gelais, R.; Guha, B.; Zhu, L.; Fan, S.; Lipson, M. Demonstration of Strong Near-Field Radiative Heat Transfer between Integrated Nanostructures. *Nano Lett.* **2014**, *14*, 6971−6975.

(23) St-Gelais, R.; Zhu, L.; Fan, S.; Lipson, M. Near-Field Radiative Heat Transfer between Parallel Structures in the Deep Subwavelength Regime. *Nat. Nanotechnol.* **2016**, *11*, 515−519.

(24) Song, B.; Thompson, D.; Fiorino, A.; Ganjeh, Y.; Reddy, P.; Meyhofer, E. Radiative Heat Conductances between Dielectric and Metallic Parallel Plates with Nanoscale Gaps. *Nat. Nanotechnol.* **2016**, *11*, 509−514.

(25) Fowler, R. H. The Analysis of Photoelectric Sensitivity Curves for Clean Metals at Various Temperatures. *Phys. Rev.* **1931**, *38*, 45−56.

(26) White, T. P.; Catchpole, K. R. Plasmon-Enhanced Internal Photoemission for Photovoltaics: Theoretical Efficiency Limits. *Appl. Phys. Lett.* **2012**, *101*, 073905.

DOI: 10.1021/acsnano.6b08597
ACS Nano 2017, 11, 3001−3009

(27) Scales, C.; Berini, P. Thin-Film Schottky Barrier Photodetector Models. *IEEE J. Quantum Electron.* **2010**, *46*, 633−643.
(28) Manjavacas, A.; Liu, J. G.; Kulkarni, V.; Nordlander, P. Plasmon-Induced Hot Carriers in Metallic Nanoparticles. *ACS Nano* **2014**, *8*, 7630−7638.
(29) Zhang, H.; Govorov, A. O. Optical Generation of Hot Plasmonic Carriers in Metal Nanocrystals: The Effects of Shape and Field Enhancement. *J. Phys. Chem. C* **2014**, *118*, 7606−7614.
(30) Sundararaman, R.; Narang, P.; Jermyn, A. S.; Goddard Iii, W. A.; Atwater, H. A. Theoretical Predictions for Hot-Carrier Generation from Surface Plasmon Decay. *Nat. Commun.* **2014**, *5*, 5788.
(31) Bernardi, M.; Mustafa, J.; Neaton, J. B.; Louie, S. G. Theory and Computation of Hot Carriers Generated by Surface Plasmon Polaritons in Noble Metals. *Nat. Commun.* **2015**, *6*, 7044.
(32) Brongersma, M. L.; Halas, N. J.; Nordlander, P. Plasmon-Induced Hot Carrier Science and Technology. *Nat. Nanotechnol.* **2015**, *10*, 25−34.
(33) Ottaviani, G.; Tu, K. N.; Mayer, J. W. Interfacial Reaction and Schottky Barrier in Metal-Silicon Systems. *Phys. Rev. Lett.* **1980**, *44*, 284−287.
(34) Hu, C. *Modern Semiconductor Devices for Integrated Circuits*; Prentice Hall: 2010.
(35) Francoeur, M.; Pinar Mengüç, M.; Vaillon, R. Spectral Tuning of Near-Field Radiative Heat Flux between Two Thin Silicon Carbide Films. *J. Phys. D: Appl. Phys.* **2010**, *43*, 075501.
(36) Joulain, K.; Mulet, J.-P.; Marquier, F.; Carminati, R.; Greffet, J.-J. Surface Electromagnetic Waves Thermally Excited: Radiative Heat Transfer, Coherence Properties and Casimir Forces Revisited in the Near Field. *Surf. Sci. Rep.* **2005**, *57*, 59−112.
(37) Naik, G. V.; Kim, J.; Boltasseva, A. Oxides and Nitrides as Alternative Plasmonic Materials in the Optical Range [Invited]. *Opt. Mater. Express* **2011**, *1*, 1090−1099.
(38) van Hest, M. F. A. M.; Dabney, M. S.; Perkins, J. D.; Ginley, D. S. High-Mobility Molybdenum Doped Indium Oxide. *Thin Solid Films* **2006**, *496*, 70−74.
(39) Guo, Y.; Molesky, S.; Hu, H.; Cortes, C. L.; Jacob, Z. Thermal Excitation of Plasmons for Near-Field Thermophotovoltaics. *Appl. Phys. Lett.* **2014**, *105*, 073903.
(40) Molesky, S.; Dewalt, C. J.; Jacob, Z. High Temperature Epsilon-Near-Zero and Epsilon-Near-Pole Metamaterial Emitters for Thermophotovoltaics. *Opt. Express* **2013**, *21*, A96−A110.
(41) Gregory, O. J.; Luo, Q.; Crisman, E. E. High Temperature Stability of Indium Tin Oxide Thin Films. *Thin Solid Films* **2002**, *406*, 286−293.
(42) Zhang, D. H.; Ma, H. L. Scattering Mechanisms of Charge Carriers in Transparent Conducting Oxide Films. *Appl. Phys. A: Mater. Sci. Process.* **1996**, *62*, 487−492.
(43) Alam, M. J.; Cameron, D. C. Investigation of Annealing Effects on Sol−Gel Deposited Indium Tin Oxide Thin Films in Different Atmospheres. *Thin Solid Films* **2002**, *420−421*, 76−82.
(44) Ordal, M. A.; Bell, R. J.; Alexander, R. W.; Long, L. L.; Querry, M. R. Optical Properties of Fourteen Metals in the Infrared and Far Infrared: Al, Co, Cu, Au, Fe, Pb, Mo, Ni, Pd, Pt, Ag, Ti, V, and W. *Appl. Opt.* **1985**, *24*, 4493−4499.
(45) Cleary, J. W.; Peale, R. E.; Shelton, D. J.; Boreman, G. D.; Smith, C. W.; Ishigami, M.; Soref, R.; Drehman, A.; Buchwald, W. R. Ir Permittivities for Silicides and Doped Silicon. *J. Opt. Soc. Am. B* **2010**, *27*, 730−734.
(46) Optical Data from Sopra Sa. http://www.sspectra.com/sopra.html (accessed 02−15−2016).
(47) Amiotti, M.; Borghesi, A.; Guizzetti, G.; Nava, F. Optical Properties of Polycrystalline Nickel Silicides. *Phys. Rev. B: Condens. Matter Mater. Phys.* **1990**, *42*, 8939−8946.
(48) Borghesi, A.; Piaggi, A.; Guizzetti, G.; Lévy, F.; Tanaka, M.; Fukutani, H. Optical Properties of Single-Crystal Titanium Disilicide. *Phys. Rev. B: Condens. Matter Mater. Phys.* **1989**, *40*, 1611−1615.
(49) Sze, S. M.; Ng, K. K. *Physics of Semiconductor Devices*; John Wiley & Sons, 2006.
(50) Murarka, S. P. Silicide Thin Films and Their Applications in Microelectronics. *Intermetallics* **1995**, *3*, 173−186.
(51) d'Heurle, F. M.; Gas, P. Kinetics of Formation of Silicides: A Review. *J. Mater. Res.* **1986**, *1*, 205−221.
(52) Tsaur, B. Y.; Weeks, M. M.; Pellegrini, P. W. Pt-Ir Silicide Schottky-Barrier Ir Detectors. *IEEE Electron Device Lett.* **1988**, *9*, 100−102.
(53) Knight, M. W.; Wang, Y.; Urban, A. S.; Sobhani, A.; Zheng, B. Y.; Nordlander, P.; Halas, N. J. Embedding Plasmonic Nanostructure Diodes Enhances Hot Electron Emission. *Nano Lett.* **2013**, *13*, 1687−1692.
(54) McKee, R. C. Enhanced Quantum Efficiency of Pd2si Schottky Infrared Diodes on < 111> Si. *IEEE Trans. Electron Devices* **1984**, *31*, 968−970.
(55) Blaber, M. G.; Arnold, M. D.; Ford, M. J. Search for the Ideal Plasmonic Nanoshell: The Effects of Surface Scattering and Alternatives to Gold and Silver. *J. Phys. Chem. C* **2009**, *113*, 3041−3045.
(56) Rakić, A. D.; Djurišić, A. B.; Elazar, J. M.; Majewski, M. L. Optical Properties of Metallic Films for Vertical-Cavity Optoelectronic Devices. *Appl. Opt.* **1998**, *37*, 5271−5283.

DOI: 10.1021/acsnano.6b08597
ACS Nano 2017, 11, 3001−3009